Published in final edited form as:
Dev Dyn. 2013 July ; 242(7): 817–831. doi:10.1002/dvdy.23969.

A Morpholino-based screen to identify novel genes involved in craniofacial morphogenesis

Vida Senkus Melvin[1], **Weiguo Feng**[1], **Laura Hernandez-Lagunas**[1], **Kristin Bruk Artinger**[1], and **Trevor Williams**[1,*]

[1]Department of Craniofacial Biology, School of Dental Medicine, University of Colorado, Denver, CO

Abstract

BACKGROUND—The regulatory mechanisms underpinning facial development are conserved between diverse species. Therefore, results from model systems provide insight into the genetic causes of human craniofacial defects. Previously, we generated a comprehensive dataset examining gene expression during development and fusion of the mouse facial prominences. Here, we used this resource to identify genes that have dynamic expression patterns in the facial prominences, but for which only limited information exists concerning developmental function.

RESULTS—This set of ~80 genes was used for a high throughput functional analysis in the zebrafish system using Morpholino gene knockdown technology. This screen revealed three classes of cranial cartilage phenotypes depending upon whether knockdown of the gene affected the neurocranium, viscerocranium, or both. The targeted genes that produced consistent phenotypes encoded proteins linked to transcription (*meis1, meis2a, tshz2, vgll4l*), signaling (*pkdcc, vlk, macc1, wu:fb16h09*), and extracellular matrix function (*smoc2*). The majority of these phenotypes were not altered by reduction of p53 levels, demonstrating that both p53 dependent and independent mechanisms were involved in the craniofacial abnormalities.

CONCLUSIONS—This Morpholino-based screen highlights new genes involved in development of the zebrafish craniofacial skeleton with wider relevance to formation of the face in other species, particularly mouse and human.

Keywords

zebrafish; craniofacial development; Morpholino; branchial arches; neural crest derived cartilages

Introduction

Development of the vertebrate face relies on a complex set of molecular, cellular and tissue interactions making this process highly sensitive to genetic and environmental perturbation. As such, abnormalities of the head, face or oral tissues are among the most common human birth defects (Chai and Maxson, 2006; Dixon et al., 2011). Cleft palate (CP), and cleft lip with or without cleft plate (CL/P), are the most frequent defects, but there are multiple

*Corresponding author UC Denver, Anschutz Medical Campus Mailstop 8120 RC-1 South Bldg, 11th floor Rm 111 12801 East 17th Ave Aurora, CO 80045 Tel. 303 724 4571 ; Fax. 303 724 4580 Trevor.williams@ucdenver.edu.

additional syndromic or non-syndromic conditions affecting other components of the craniofacial skeleton. The genetic underpinnings of many such craniofacial abnormalities remain to be uncovered. Previous studies have demonstrated that the molecular pathways involved in human craniofacial development are conserved across numerous species, including mouse, chick, *Xenopus*, and zebrafish and studies in these model organisms have complemented human genetic analyses and broadened our understanding of the molecular pathways involved in craniofacial development (Chai and Maxson, 2006; Schilling and Le Pabic, 2009; Szabo-Rogers et al., 2010; Curtin et al., 2011; Dixon et al., 2011;Ferretti et al., 2011; Swartz et al., 2011; Weiner et al., 2012).

The zebrafish (*Danio rerio*) is one of the more significant experimental systems to study the environmental and genetic factors influencing craniofacial development, in part due to its relatively low cost, readily-visualized embryogenesis and ease of manipulation. Thus, this species has been used in several forward genetic screens using ENU or viral based mutagenesis methods for the identification of novel craniofacial mutations (Neuhauss et al., 1996; Piotrowski et al., 1996; Schilling et al., 1996; Amsterdam et al., 1999; Wang et al., 2007). The possibility of performing reverse genetic studies in zebrafish has also been accelerated with the use of anti-sense Morpholino, TILLING, Zinc finger nuclease and TALEN technologies (reviewed in (Lawson and Wolfe, 2011;Moore et al., 2012)).

Recently, we used microarray analysis to identify and catalog transcripts expressed in the developing mouse face (Feng et al., 2009). Among this dataset we identified numerous genes that showed high-level or dynamic spatial/temporal expression patterns and were either completely novel or had no previously known function in craniofacial development. Such genes included proteins predicted to be involved in cell adhesion, extracellular matrix composition, transcriptional regulation or cell signaling (Feng et al., 2009). We theorized that if orthologs of these genes were conserved in both sequence and in expression pattern between the mouse and zebrafish lineages then these genes might represent important candidates for conserved regulators of facial development. We tested this hypothesis by performing an in depth analysis of the function of *Vgll2*, a gene we had determined was highly expressed during development of both mouse and zebrafish facial structures. Gene knockdown of *Vgll2* in the zebrafish produced major craniofacial phenotypes and indicated the utility of this approach for highlighting new genes involved in face formation (Johnson et al., 2011). Therefore, in the current study, we first identified a set of genes that showed similar expression in the embryonic head between mouse and zebrafish. We then conducted a Morpholino-based reverse genetic screen in the zebrafish as a rapid means to assess the function of this gene set in vertebrate facial development. These studies provide a new paradigm to study craniofacial development and demonstrate the power of combining bioinformatic analysis with reverse genetic analysis.

Results

General Approach

We identified zebrafish orthologs of mouse candidate genes by subjecting mouse gene sequences to BLAST analysis against zebrafish protein and transcript (RefSeq and EST) databases. Of the >80 mouse genes we analyzed, ~75% had readily identifiable zebrafish

orthologs (Table S1). In some cases, continued refinement of the zebrafish genome sequence led to orthologs being identified after we had concluded our analyses; these were not included in the Morpholino-based screen (Table S1). Additionally, for some mouse candidates, we identified two zebrafish orthologs of high sequence homology, presumably due to a genome duplication associated with the evolution of the teleost lineage (reviewed in (Volff, 2005)). In general, the large number of identifiable zebrafish orthologs to our mouse candidate genes supports the idea that genes expressed in the mouse face during craniofacial development are conserved across vertebrate species.

To assess the role of candidate genes in craniofacial development, we first analyzed gene expression patterns in the zebrafish by a combinatorial approach using both *in silico* and *in situ* hybridization techniques. Initially, we searched for data relating to candidate gene expression in the published literature and on the ZFIN website (Thisse et al., 2001). Next, for those genes with no previously available expression data, *in situ* hybridization analysis was performed. Genes that showed expression patterns in the developing head (pharyngeal arches, neural crest, etc.) between 12 and 48 hours post-fertilization (hpf) were selected for further functional analysis (Table 1 and Table S2). To determine whether this group of >40 candidate genes were functionally important for zebrafish craniofacial development, gene-specific Morpholinos (MOs) were designed and injected to 1-cell stage zebrafish embryos. Morpholino-injected zebrafish embryos were examined at 24 and 48 hpf for gross morphological defects to determine effective MO dose and to eliminate genes from the screen that caused widespread early embryonic defects, such as gastrulation failure. Subsequently, morphant larvae that passed this screening step were fixed at 5 or 6 days post-fertilization (dpf) and analyzed for craniofacial anomalies. Morphant larvae were compared to clutch-mates by gross external examination as well as by alcian blue and alizarin red staining for analysis of cartilage and bone structures. Figure 1 shows representative images of wild-type larvae both before (Figure 1A) and after (Figure 1B-E) skeletal staining.

The wild-type zebrafish head skeleton has two major components that can be separated by dissection and examined in isolation: (1) the viscerocranium which is formed by Meckel's cartilage and palatoquadrate of the lower jaw, as well as the hyosymplectic, ceratohyal, and gill-forming ceratobranchial cartilages (Figure 1D); and (2) the neurocranium, consisting of the base of the skull, including the ethmoid plate, trabeculae and parachordals (Figure 1E). The entire viscerocranium and the anterior aspect of the neurocranium are derived from neural-crest cells while the posterior aspect of the neurocranium is mesodermal in origin (Schilling and Kimmel, 1994; Wada et al., 2005; Eberhart et al., 2006). In addition to cartilages, we were also able to assess the effect of MO injection on formation of early bone structures (Figure 1D, arrowheads) and the inner ear ossicles at 5 and 6 dpf (Figure 1E, arrow). We did not identify any morphants that demonstrated specific bone or pharyngeal tooth phenotypes, however, we did not examine morphants after 6 dpf to determine whether any of the gene candidates were involved in later bone development.

From the original set of >40 genes, we chose to concentrate on 8 genes that gave consistent craniofacial phenotypes (Table 1). Details on the entire gene set we examined are summarized in Tables S1 and S2. For each of the 8 genes in Table 1, we generally first employed a translation-blocking MO (ATG or UTR), if an initiator codon was identifiable.

Next, a splice-blocking MO (SPL; Table 1 and Table S2) was used as a second method of gene knockdown. In certain instances, for example when no initiator codon was apparent in the draft zebrafish database sequences, two independent SPL MOs targeting different regions of the gene were utilized. Since most of the candidate genes were novel or relatively uncharacterized in zebrafish, there were no immunological reagents to monitor changes in gene expression at the protein level; however, we assessed the efficacy of the splice blocking MOs to alter gene expression by examining changes in the RNA transcript (Figure S1). In the final step of our analysis, we assessed the role of *p53*-mediated apoptosis in the craniofacial phenotype by injecting experimental MOs into *p53* null zebrafish embryos or co-injecting a *p53*-specific MO (Table 1). This was a critical step in our studies as MOs have been previously shown to elicit craniofacial defects through induction of cell death in the hindbrain, an important source for cranial neural crest cells (Robu et al., 2007).

For the 8 genes we fully analyzed (Table 1), the craniofacial phenotypes could be segregated into three groups according to the structures that were primarily altered in the morphants. These were: (I) genes that were essential for formation of the ventral viscerocranium; (II) genes that were essential for the development of the anterior neurocranium; and (III) genes that were critical for general morphogenesis of all neural crest-derived structures, including those of both the viscerocranium and neurocranium.

Class I Phenotypes—The class I genes were primarily involved in the formation and/or patterning of the ventral viscerocranial cartilages and comprised three genes: *smoc2*, *meis1*, and *meis2a*. Expression data for these three genes is included in Supplementary Figure 2 (A-F).

smoc2—*SPARC-related modular calcium-binding protein 2* (*Smoc2*) encodes an extracellular matrix protein that is known to modulate cell division, attachment and response to growth factors (Vannahme et al., 2003; Rocnik et al., 2006; Liu et al., 2008; Maier et al., 2008; Liu et al., 2009). Expression of *mouse Smoc2* increases in all three craniofacial prominences between E10.5 and E12.5 (Feng et al., 2009) and transcripts can be detected in the developing face, limbs and somites at E12.5 (Liu et al., 2008). The single zebrafish *smoc2* homolog (Table 1) shows ~67% amino acid identity with the mouse protein sequence (http://www.ncbi.nlm.nih.gov/). In zebrafish embryos, expression of the *smoc2* transcript can first be detected in the branchial arches between 30 and 42hpf and is apparent in the tooth germs and pharyngeal endoderm later in development (up to 72hpf) ((Thisse et al., 2001 ; Bloch-Zupan et al., 2011) and see Supplementary Figure 2A, B).

Injection of a translation blocking MO to the 5′ UTR of *smoc2* induced alterations in the viscerocranial cartilages in 30% of morphants. Approximately 10% of the affected UTR morphants (3% of total injected larvae) had a smaller head and eye abnormalities as compared to uninjected controls (Figure 2A and see Figure 1 throughout for equivalent wild-type appearance). The remaining UTR morphants completely lacked eyes, had severely reduced head size (Figure 2A, inset) and lacked all head cartilage (Figure 2D, inset). Injection of a splice-blocking MO (SPL) targeted to the splice donor site for exon 11 of *smoc2* induced hypoplasia of the head and eye abnormalities in 50-60% of injected fish (Figure 2B). Skeletal staining showed that, when compared with an uninjected control

(Figure 2C), the ceratohyals of both the UTR and SPL morphants were flattened or inverted (Figure 2D, E). In addition, morphant ceratobranchials (CBs) were reduced in both size and number, with loss of the most posterior CBs. To determine if the SPL MO disrupted splicing, RNA pools isolated from *smoc2* morphants were utilized for RT-PCR analysis using primers spanning the targeted exons. This analysis indicated that the SPL MO significantly altered the processing of *smoc2* RNA (Figure S1A), strongly suggesting that the observed craniofacial phenotypes are due to loss of wild-type *smoc2* transcripts.

Meis genes—From our array studies, two homeodomain genes, *Meis1* and *Meis2*, showed dynamic expression in the developing mouse face (Feng et al., 2009). *In situ* hybridization demonstrates a distinctive expression pattern for both *Meis1* and *Meis2* in the lamboidal junction (http://embrys.jp/embrys/), a feature of E10.5 mouse embryos in which the maxillary and nasal prominences meet in a characteristic lambda shape. In zebrafish, we identified a single *Meis1* ortholog -*meis1*, with 95% amino acid identity to the mouse protein (http://www.ncbi.nlm.nih.gov/). There were two orthologs for *Meis2* - *meis2a* and *meis2b* with 88% and 96% identity to the mouse protein, respectively (http://www.ncbi.nlm.nih.gov/, Table 1 and Table S2). All three of these genes are expressed in the branchial arches of 48hpf zebrafish embryos ((Thisse and Thisse, 2005) and see Supplementary Figure 2C-F).

Injection of a translation-blocking MO to *meis1* induced a reduction in the ventral region of the zebrafish head at 5dpf (Figure 3A). A comparison of the underlying skeletons of control (Figure 3B) and morphants (Figure 3C-E) revealed that approximately 50% of *meis1* morphants had varying degrees of viscerocranial cartilage fusions and occasionally ectopic cartilages. Cartilage fusions occurred between skeletal elements derived from the same or adjacent branchial arches; as shown in Figure 3C and D, the arch 1 derivatives, Meckel's and palatoquadrate, were fused together and also fused to the arch 2 derived hyosymplectic (see also Supplementary Figure 3B). Similarly, the arch 2-derived ceratohyal was fused to ceratobranchial cartilages derived from the adjacent arch 3 domain (Figure 3C, indicated by asterisk, and Supplementary Figure 3B) and frequently ceratobranchial cartilages derived from adjacent arches were also fused to each other (Figure 3E). The cartilages of the viscerocranium were in some cases misshapen, being broader and misaligned with each other possibly as a result of fusion. For example, the palatoquadrate sometimes had a flatter and wider appearance in ventral view suggesting that it had been rotated on its long axis from its normal position (Figure 3C and Supplementary Figure 3A-C').

Next, we injected a splice blocking MO targeted to the exon1-intron1 boundary of *meis1*. When used in isolation, even at the highest dose of 20ng, this reagent did not generate the facial defects obtained with the ATG MO (Figure 3F). We therefore combined 20ng of the SPL MO with a sub-optimal dose of the *meis1* ATG MO (2ng) to determine whether this combination could evoke a craniofacial phenotype. At these doses, the individual MOs did not induce cartilage fusions in greater than ~5% of morphants (Figure 3F and data not shown). However, when injected together, >30% of morphants exhibited the cartilage fusion phenotype similar to higher doses of the ATG MO alone (Figure 3G). These data demonstrate that the two MOs can cooperate to inhibit *meis1* activity and provide further support for a role for *meis1* in zebrafish craniofacial development. Moreover, we determined

that the *meis1* transcript was not processed appropriately in the presence of the SPL MO and generated a larger product in which the first intron was retained (Figure S1B). We suspect that the specific level of gene knockdown we observed was not sufficient to generate a robust morphant phenotype unless normal protein levels were further reduced by the addition of small amounts of the ATG MO.

Next, translation blocking MOs were injected against either *meis2a* or *meis2b*. Analysis of morphants indicated that an abnormal phenotype was only produced with *meis2a* and therefore further analysis was focused on this gene. The *meis2a* ATG morphants resembled *meis1* morphants in that they had recessed lower jaws as well as fusions of viscerocranial cartilages and ectopic cartilage (compare Figure 3A to H, and C to I). Similar to *meis1*, the cartilages of *meis2a* morphants were also broadened and misshapen with ectopic cartilages present usually along the midline (Figure 3J). However, in contrast to the *meis1* phenotype, *meis2a* morphants frequently displayed a full fusion of all arch 1 elements (Meckel's and palatoquadrate) with the ceratohyals resulting in the formation of a single "D"-shaped cartilaginous element (Figure 3I and Supplementary Figure 3D-E). The first ceratobranchial cartilage was often also fused to this D-shaped cartilage (Figure 3I and Supplementary Figure 3E). Note that we tested a number of SPL MO targeted to *meis2a* to provide independent confirmation of the ATG MO results, but have not yet identified a splice blocking MO that will interfere with normal *meis2a* RNA processing. Nevertheless, the finding that MOs targeting the zebrafish *meis* gene family produced similar phenotypes provides strong evidence for a role of these genes in craniofacial morphogenesis.

Class II phenotypes—Class II phenotypes encompass those genes that are important for patterning the anterior neurocranium, including the ethmoid plate and trabeculae. There was one gene that consistently fell within this classification: *wu:fb16h09*. This gene is the zebrafish ortholog of mouse neuron-derived neurotrophic factor (Ndnf, GeneID: 68169; previously termed *A930038C07Rik)* with which it shares ~75% amino acid sequence identity (http://www.ncbi.nlm.nih.gov/). In our mouse microarray screen, *A930038C07Rik* was identified as an uncharacterized gene that was expressed in the facial prominences, particularly the maxillary and to a lesser extent the mandibular prominence, as well as along the neural tube (Feng et al., 2009). Analysis of *wu:fb16h09* expression at 24 and 48hpf (Fig 4A-D) indicated that, in common with the mouse ortholog, transcripts derived from this zebrafish gene could be detected in the ventral CNS (or floorplate), somites at the midline and the hypochord (Fig4A, B) and around the stomodeum in a region ventral to the eye (Figure 4C and D). Additional expression of *wu:fb16h09* was observed in a region consistent with the presumptive trigeminal ganglia and posterior cranial ganglia (Figure 4C).

Zebrafish injected with a MO targeted to either the ATG or the intron 3-exon 4 splice junction (SPL) of *wu:fb16h09* produced similar phenotypes. Specifically, both types of morphants had a reduction of the most rostral aspect of the head (Fig 4E, arrowhead), but had normal body length and did not appear developmentally delayed as judged by the size and shape of the yolk. Skeletal staining of control (Figure 4F) and morphant (Figure 4G and H) larvae at 5dpf demonstrated that the rostral tips of the trabecular cartilages of the neurocranium were fused in 100% of abnormal fish and the ethmoid plate was reduced or absent. At higher MO doses the entire neural crest derived neurocranium – both ethmoid

plate and trabeculae - was absent (data not shown). Additionally, some morphants exhibited small spurs that protruded laterally from the trabeculae (data not shown, but also see Figure 7A). In ATG morphants, the viscerocranium appeared normal (data not shown, 100%), but the splice MO did elicit a reduction of the viscerocranial cartilages (Figure 4G). We also detected alterations in *wu:fb16h09* RNA in the SPL morphants, with a clear increase in the unspliced or abnormally spliced products containing intron 3 sequences (Figure S1C). The large size of associated intron sequence (9.8Kb) made cloning and sequence analysis of the mis-spliced products problematic, but nevertheless the SPL morphant clearly disrupts *wu:fb16h09* mRNA processing, consistent with the observed morphant phenotypes.

Class III phenotypes—MO knockdown of the Class III genes caused a shared phenotype of progressive and dose-dependent loss of the viscerocranium and the neural-crest derived cartilages of the anterior neurocranium. Four genes belonged to this category - *Macc1*, *Vgll4l*, *Tshz2* and *Pkdcc* - none of which have been extensively studied previously in the zebrafish system. Data on the expression of these genes is shown in Supplementary Figures 2 and 4.

Macc1 (metastasis associated with the colon cancer 1)—*Macc1* encodes an SH3-domain containing protein that is predicted to act in signal transduction, stimulating proliferation and cell migration, although its exact mechanism of action is unclear (Stein et al., 2009). In E10.5 mouse embryos, we detected *Macc1* expression in the ectoderm of the mandibular and maxillary prominences as well as the ectoderm and mesenchyme of the frontonasal prominences (Figure 5A and data not shown). A BLAST analysis of the zebrafish genome using the mouse *Macc1* mRNA sequence yielded a single ortholog with ~45% sequence identity (http://www.ncbi.nlm.nih.gov/ and Table 1). *In situ* hybridization of 24hpf zebrafish embryos demonstrated that *macc1* was expressed in the brain, eye, otic vesicle and pronephros (Supplementary Figure 4A). Otic vesicle expression continued at 48hpf and *macc1* transcripts became apparent in the developing stomodeum (Figure 5B and B', ventral view).

With available sequence data we were unable to design an effective ATG MO, therefore we focused our efforts on two SPL MOs targeted to two different splice junctions of *macc1* that produced identical phenotypes (Table 1). Externally at 5dpf, *macc1* morphants showed a collapse of the rostral aspect of the head and eye abnormalities (Figure 5C). Both *macc1* SPL MOs altered *macc1* mRNA splicing as measured by RT-PCR (Figure S1D). The SPL1 MO targeted the intron 2-exon 3 splice acceptor and produced a message that included intron 2 (Figure S1D top). Injection of SPL2 MO, which targeted the exon 2-intron 2 splice donor, caused deletion of the 168 nt exon 2 (Figure S1D bottom). This deletion would alter the N-terminus of the protein, but since this sequence is not as well conserved as more C-terminal residues between species we suspect this accounts for the lower percentage mutant phenotype observed with the SPL2 MO. In this respect, for over 120 embryos injected for each MO, SPL1 and SPL2 produced ~66% and 10% of abnormal larvae, respectively.

Alcian blue staining of control (Figure 5D), *macc1* SPL1 or SPL2 morphants (Figure 5E and F) revealed that at lower doses of MO the viscerocranial cartilages were hypoplastic or lost. This included severe reduction or complete loss of the ceratobranchials (Figure 5E and F,

asterisk), a flattening or inversion of the angle between the paired ceratohyal cartilages (Figure 5E and F, arrowhead), and smaller Meckel's and palatoquadrate cartilages resulting in a recessed lower jaw (Figure 5E, arrow). In severely affected morphants, the majority of the viscerocranial cartilages were absent and the ethmoid plate and trabecular cartilages of the neurocranium were severely reduced or absent (Figure 5E' and F'). Interestingly, the posterior cartilages of the neurocranium, including the parachordals, were usually present in *macc1* morphants, but were malformed in most extreme morphant phenotypes suggesting a possible interaction between the neural crest and mesoderm-derived tissues (Figure 5E' and F').

Vgll4l—The mouse vestigial-like ortholog *vestigial-like 4* (*Vgll4*) was identified in our microarray dataset as expressed in all 3 prominences during craniofacial development (Feng et al., 2009). Two *Vgll4* orthologs occur in zebrafish, *vgll4* and *vgll4l*, which show 68% and 31% sequence identity to the mouse protein, respectively (http://www.ncbi.nlm.nih.gov/, Table 1 and Table S2). In our initial screens targeting both genes with specific ATG MOs, *vgll4* morphants displayed only a minor craniofacial phenotype at the highest MO doses, while *vgll4l* morphants displayed a distinct mutant phenotype (Figure 6A, D, E and data not shown). Therefore we concentrated on the *vgll4l* ortholog for further analysis. Previous analysis has shown that *vgll4l* is expressed in the developing zebrafish head (Thisse et al., 2001). During early somitogenesis, *vgll4l* is expressed at the neural plate border, an important source of neural crest cells that populate the future face (Thisse et al., 2001). At 24hpf and 48hpf, *vgll4l* is found expressed primarily in the endodermally derived pharyngeal pouches (Supplementary Figure 2G, H and (Thisse et al., 2001)).

Both ATG and SPL morphants for *vgll4l* displayed a collapse of the rostral aspect of the zebrafish head along with a gaping lower jaw (Figure 6A and data not shown). Unlike *macc1*, *vgll4l* morphants did not have any obvious eye abnormality (compare Figure 5C and 6A). The *vgll4l* SPL MO targeted the splice acceptor site of exon 5 and resulted in transcripts that included intron 4 (Figure S1E). In comparison to controls (Figure 6B, C) knockdown of *vgll4l* produced hypoplasia of the viscerocranium in mild morphant larvae with flattening or complete inversion of the ceratohyal cartilages and loss or partial loss of ceratobranchials (Figure 6D and E). The ethmoid plate of mild *vgll4l* morphants was also reduced in size (Figure 6D and E). Severe *vgll4l* morphants displayed complete loss of all viscerocranial cartilages and anterior neurocranial cartilages were further reduced or were completely absent (Figure 6D' and E'), a phenotype similar to that observed for *macc1* (Fig 5).

Tshz2—All three mouse teashirt homologs, *Tshz1-3*, show increasing expression levels in the developing mouse face between E10.5 and E12.5 with *Tshz1* more highly expressed in the mandibular prominence and *Tshz2* and *Tshz3* expressed at equal levels over all three prominences (Feng et al., 2009). Mouse knock-outs for *Tshz1* and *Tshz3* have been extensively analyzed and display defects in multiple developmental systems including the face and brain (Core et al., 2007;Caubit et al., 2008; Caubit et al., 2010). Less is known about *Tshz2* in mouse although preliminary analysis of a *Tshz2* gene trap termed TM67

indicated a post-natal growth deficiency of unknown etiology (Horie et al., 2003), and this led us to focus on the role of *Tshz2* in zebrafish craniofacial development.

In zebrafish, we identified a single *Tshz2* ortholog, *tshz2* (Table 1), which showed 56% amino acid identity to the mouse protein (http://www.ncbi.nlm.nih.gov/). Previous studies have shown that *tshz2* is expressed in the zebrafish branchial arches at 24hpf ((Santos et al., 2010) and see Supplementary Figure 4). Injection of a translation blocking ATG MO or a SPL MO targeted to the exon 2 splice acceptor of *tshz2*, caused collapse of the anterior-most part of the head as was observed for the other Class III genes (Figure 6F and data not shown). Subsequent alcian blue staining demonstrated that in mild *tshz2* morphants the ceratobranchials were typically absent, the ceratohyal was flattened or inverted (Figure 6G and H) and in some cases the Meckel's, palatoquadrate and hyosymplectic cartilages were severely misshapen (Figure 6H). In addition, the ethmoid plate was reduced or absent (Figure 6G and H). The majority of severe *tshz2* morphants displayed a complete loss of the viscerocranium (Figure 6G' and H'), but in occasional larvae a small viscerocranial cartilage could be observed (Figure 6G', arrowhead). The ethmoid plate of severe *tshz2* morphants was absent with fusion of the trabeculae (Figure 6G' and H', asterisk). Although the SPL MO produced phenotypes that were nearly identical to that of the ATG MO, we were unable to detect changes in the *tshz2* transcript. This may be due to the fact that *tshz2* contains only two exons with an intervening intron of more than 50 kb making identification of mis-spliced transcripts difficult using standard techniques (http://www.gene-tools.com/).

Pkdcc (AW548124)—In our mouse microarray analysis, we identified *AW548124* as a gene with increasing high level expression in the developing face (Feng et al., 2009). This gene, now termed *Pkdcc* but also known as *Vlk* in both mouse and human, encodes a putative protein kinase (Imuta et al., 2009). In E9.5 mouse embryos, expression of *Pkdcc* has been detected in the mesenchyme of the branchial arches, consistent with our previous findings, as well as in the limb buds (Imuta et al., 2009; Kinoshita et al., 2009). Examination of the zebrafish databases indicated that there are two *Pkdcc* orthologs (Table1 and Table S2), termed *vlk* and *LOC565254* which encoded proteins with ~56% and 40% amino acid identity to mouse Pkdcc, respectively (http://www.ncbi.nlm.nih.gov/). Here we refer to *LOC565254* as zebrafish *pkdcc*, and we have obtained similar craniofacial defects using two independent MOs that target this transcript. The ATG morphants showed rostral collapse of the head along with eye abnormalities and an enlarged yolk possibly indicating a developmental delay (Figure 6I). Alcian blue staining for cartilage defects demonstrated that mild morphant phenotypes included loss of ceratobranchial cartilages with inversion of the ceratohyal (Figure 6J). More severe *pkdcc* ATG morphants lacked all but a few fragments of the viscerocranial cartilages (Figure 6J', arrowhead) and had a severely truncated ethmoid plate. The *pkdcc* SPL morphants showed similar mild and severe cartilage phenotypes as ATG morphants (Figure 6K and K'). The SPL MO targeted the exon 4 splice donor and produced several aberrant transcripts that would be predicted to compromise pkdcc protein function (Figure S1F) consistent with the occurrence of morphant phenotypes.

We have also employed various MOs to target *vlk*, but to date we have only obtained consistent craniofacial phenotypes with a SPL MO targeted to the splice donor of exon 3. Molecular analysis indicated that the SPL MO resulted in aberrant transcripts containing

>2kb of intron 3 sequence (data not shown). The SPL morphants displayed reduced head size and cartilage defects similar to other Class III genes, including reduction of viscerocranial cartilages in mild phenotypes and complete loss of the viscerocranium with reduced neurocranium in more severe phenotypes (Supplementary Figure 5). Taken together, the correlation of the *vlk* SPL MO morphant cartilage defects with disruption of *vlk* RNA processing provides further evidence that these two zebrafish *Pkdcc* orthologs may both regulate facial development.

The Role of p53 in Morphant Phenotypes—Previous studies have demonstrated that injection of MOs can induce non-specific activation of *p53*-dependent apoptosis in the hindbrain (Robu et al., 2007; Gerety and Wilkinson, 2011). Because the hindbrain is a source of neural crest cells that populate the pharyngeal arches, these off-target effects can result in loss of neural-crest derived cartilages, reminiscent of the Class III phenotypes we describe in the present study. These observations led us to assess the role of *p53*-mediated apoptosis in morphants for all eight genes under analysis. The gene specific MOs were either injected into *p53*-mutant zebrafish (Berghmans et al., 2005) or co-injected into wild-type embryos with a MO targeted to *p53* (Robu et al., 2007). The morphant phenotypes for the majority of the genes analyzed were unaltered by loss or reduction of *p53* indicating that the resulting phenotypes are not related to *p53* dependent apoptosis (Table 1, Supplementary Figure 6, and data not shown). The exceptions were the Class II gene *wu:fb16h09* (Figure 7A, B) and the Class III gene *pkdcc* (Figure 7C, D), for which loss of *p53* rescued the craniofacial phenotypes associated with ATG MO injection (Figure 7). These findings indicate that these two morphant phenotypes are dependent on *p53*-mediated developmental mechanisms for their expressivity (see Discussion).

Discussion

We previously generated datasets that investigated the gene expression changes associated with mouse craniofacial development (Feng et al., 2009). Here, we have chosen mouse genes with dynamic expression patterns and examined their potential function in craniofacial development using a reverse genetic approach in the zebrafish. Our MO-based studies identified a number of genes and gene families that alter zebrafish craniofacial formation. All told, from an original dataset of >80 mouse genes, we screened ~40 zebrafish genes by MO-based targeting (summarized in Table S1). In general, our first approach was to screen each candidate gene with a MO that would be predicted to inhibit translation (Table 1 and Table S2). Genes that failed to produce a consistent craniofacial morphant phenotype using this approach were generally not pursued further and included those phenotypes showing embryonic lethality prior to 48hpf with a reduction or complete loss of somites, no yolk extension and a shortened body axis. These latter phenotypes have been previously associated with defects in early embryogenesis and gastrulation (Hammerschmidt et al., 1996) and in our analysis the genes in this subclass were *adap1*, *ribosomal protein S6 kinase like (RPS6kaI)* and *1810019J16Rik* (Table S2, Figure S7 and data not shown).

The 11 genes for which a first MO produced a craniofacial defect were then extensively analyzed using additional MOs that would be predicted to inhibit mRNA processing. In general, only those genes that produced affected larvae with both MO approaches were

included in our final analysis of morphant phenotypes (8 genes, Table 1 and (Johnson et al., 2011)). We classified these genes into three groups according to craniofacial cartilages that were altered in morphant larvae – viscerocranium only (Class I), primarily neurocranium (Class II) and all neural crest-derived cartilages (Class III).

Class I morphants exhibited defects only in the viscerocranial cartilages- derived from the pharyngeal arches and were represented by *smoc2*, *meis1* and *meis2a* (Figures 2 and 3). There are two highly related *Sparc related modular calcium binding* genes in vertebrates, *Smoc1* and *Smoc2*, which encode extracellular matrix proteins that modulate cellular responses to extracellular signals, particularly BMPs (Vannahme et al., 2003; Rocnik et al., 2006; Liu et al., 2008). During craniofacial development, signaling molecules, such as FGF, BMP, Shh and Wnt have critical functions in growth and patterning of the face. As such, factors that promote or inhibit ligand-receptor interactions or alter receptor signaling also have a potential regulatory function in craniofacial development. Recently, mutations in *SMOC2* have been associated with developmental defects in dentition of both humans and zebrafish (Bloch-Zupan et al., 2011). We note that craniofacial defects were apparent in these previous zebrafish studies, but were not analyzed. Here, we show that inhibition of *smoc2* caused a reduction in head size and alteration in the viscerocranial skeleton of zebrafish, in addition to eye abnormalities. We did not pursue any dental defects, but note that alteration of dentition was not a consistent phenotype in our *smoc2* morphants. Some morphants maintain dentition even in the absence of normal ceratobranchial development, while other morphants lack larval teeth at 5dpf (Figure 2). Intriguingly, the related human gene *SMOC1* has been linked to Waardenburg anophthalmia syndrome in humans (Abouzeid et al., 2011; Okada et al., 2011). Like *Smoc2*, *Smoc1* is also expressed in the developing mouse face and gene targeting of *Smoc1* in mice resulted in coloboma and microphthalmia as well as a significant incidence of cleft secondary palate (Okada et al., 2011; Rainger et al., 2011). Previously, *smoc1* morphants have also been generated in zebrafish and found to have microphthalmia and gross defects in craniofacial morphology, but the latter alterations were not investigated in detail (Abouzeid et al., 2011). The observation that inhibition of either of these two zebrafish *smoc* genes results in craniofacial defects suggests wider roles for these two genes in regulating vertebrate facial development. In the future it will be interesting to determine whether compound mutants reveal a redundant or combinatorial function in craniofacial development as well as investigating a possible role for *SMOC2* in additional cases of human Waardenburg anophthalmia syndrome that do not map to *SMOC1*.

Meis genes are members of the TALE homeodomain family and interact with the Pbx DNA binding co-factors to modulate the expression of *Hox* target genes (Moens and Selleri, 2006). All told, we targeted the expression of five members of this gene family that are expressed in the zebrafish neural crest and branchial arches (Thisse and Thisse, 2005). *Meis1* and *meis2a* morphants shared similar craniofacial phenotypes, whereas the MOs we targeted to *meis2b*, *meis3*, and *meis4* did not affect the developing face (Figure 3 and data not shown). *Meis1* and *meis2a* morphants were typified by fusions of cartilages from adjacent arches suggesting failed separation of migrating neural crest cell streams. These phenotypes are reminiscent of those caused by loss of *Pbx1* in mouse or *pbx4 (lazarus)* in

zebrafish, which include absence of hindbrain segmentation as well as fusions and transformations of the neural crest-derived cranial cartilages (Popperl et al., 2000; Selleri et al., 2001; Ferretti et al., 2011). To date, analyses of mouse *Meis* gene function have not included extensive craniofacial analysis, however, human genetic mapping studies have indicated a potential link between *MEIS2* and craniofacial clefting (Crowley et al., 2010). Therefore, further studies of the role of this gene family in vertebrate development, as well as any potential genetic interactions with *Pbx* partners, appears warranted.

We also determined that *lix1l*, a relatively uncharacterized gene, could be also be provisionally placed into Class I (Table S2 and Supplementary Figures 4 and 5A). Zebrafish treated with a *lix1l* ATG MO exhibited loss of ceratobranchials and an inversion of the ceratohyal, a phenotype unaltered by loss of *p53* (data not shown). While we were unable to identify a second Morpholino that phenocopied the ATG MO, the preliminary expression data and morphant phenotypes suggest that *lix1l* can function in craniofacial development.

Class II genes affected primarily the neurocranium and we studied one such gene in detail, *wu:fb16h09* (Figure 4). In addition, preliminary studies indicate that *pcdh19* may also fit into this category based on the results obtained using an ATG MO, although we have not been able to identify a second MO that recapitulates these findings (Table S2 and Supplementary Figure 5). The phenotypes associated with these class II morphants are similar to a subclass of zebrafish ENU-induced mutants that have mid-line defects. A number of these ENU mutants have been mapped to components of the sonic hedgehog (*shh*) and wingless (*wnt*) signaling pathways. In particular, the *you-too* (*yot)* mutation in *gli2a* and the *silberblick* (*slb*) mutation in *wnt11* have trabecular fusions and truncation or aplasia of the ethmoid plate that phenocopy the class II phenotypes observed in our screen (Brand et al., 1996; Kimmel et al., 2001; Eberhart et al., 2006). The craniofacial defects associated with the midline group may not result from a defect in cartilage forming cells, but instead may be caused by changes in the neurectoderm or prechordal plate (Kimmel et al., 2001). Additional studies in chick and mouse have also indicated that factors produced within the CNS, including Shh, can also act directly on facial patterning (Hu and Marcucio, 2009). Interestingly, the class II genes we analyzed are expressed in the developing zebrafish brain (Figure 4 and Supplementary Figure 4) and we hypothesize that the neurocranial defects may be secondary to a brain patterning defect. Indeed, in zebrafish, previous MO-targeting of *pcdh19* indicated that it was required for neurulation via its interactions with N-cadherin (Emond et al., 2009; Biswas et al., 2010). Similarly, the human ortholog of *wu:fb16h09*, previously known as *c1orf31*, has been renamed *NDNF* based on a possible function as a neurotrophic factor in the CNS (Kuang et al., 2010).

In zebrafish, the neurocranium not only supports the brain as the base of the skull, but also acts as the upper jaw (Figure 1) and is derived from neural crest cells that migrate anterior to the eye. In contrast, the mammalian upper jaw forms from the fusion of the paired maxillary prominences with the nasal prominences. Recent studies now show that at least some of the genetic programs that govern palatogenesis in mice are conserved in zebrafish suggesting that the upper jaw of mammals may be homologous to the anterior neurocranium of zebrafish (Eberhart et al., 2008; Swartz et al., 2011). Therefore, one prediction is that the class II genes may influence development of the maxillary prominences and palatal shelves

in the mouse model. In this respect, expression of the mouse homologue of *wu:fb16h09*, *Ndnf* (*A930038C07Rik)*, is high in the maxillary prominence (Feng et al., 2009) suggesting a role in upper jaw development.

Knockdown of the Class III genes *macc1*, *vgll4l*, *tshz2*, *pkdcc* and *vlk* produced the third group of morphant phenotypes, a progressive and MO-dose dependent loss of neural crest derived cartilages (Table 1, Figures 5, 6, Supplementary Figure 5C, and Table S2). The loss of primarily neural crest-derived cartilages suggests an important role for Class III genes in this cell type since zebrafish mutants in genes important for neural crest cell specification and survival, such as *sox9*, also have similar phenotypes (Yan et al., 2005). Studies on an additional class III gene, *vgll2*, that served as the prototype for our screening strategy supports this conjecture as we determined that it was required for endodermal pouch morphogenesis and neural crest survival (Johnson et al., 2011). Additionally, mice deficient in *Pkdcc* exhibit palatal clefting possibly as a result of deficiencies in neural crest-derived mesenchymal cells (Imuta et al., 2009; Kinoshita et al., 2009). Moreover, loss of mouse *Tshz1* results in clefting of the secondary palate and malformations of other neural crest derived structures of the middle ear supporting a conserved role for the *Tshz* family in neural crest function (Core et al., 2007). We also note that mice carrying a transposon-tagged *Tshz2* insert have been described although the effect of the mutation on *Tzhz2* function has not been clarified (Horie et al., 2003). Homozygous mutant mice are significantly smaller than their wild-type littermates (Horie et al., 2003), and we suggest that further analysis of the craniofacial organization in these mice would be informative.

Finally, it has been proposed that zebrafish phenotypes similar to the Class III defects described here are caused by MO-induced, non-specific upregulation of the p53 apoptotic pathway. Therefore, we examined if the various morphant phenotypes we had obtained were altered when *p53* levels were reduced. We determined that the majority of the gene knockdowns were unaffected by *p53* status, with the exception of the Class II gene *wu:fb16h09* and the Class III gene *Pkdcc* (Figure 7). In these latter two instances, the morphant phenotype reverted to a more wild-type condition upon inhibition of p53, suggesting that the phenotype was dependent upon *p53*-mediated apoptosis. However, two lines of evidence argue against the morphant phenotypes we describe being caused by non-specific effects of the MOs. First, *wu:fb16h09* knockdown induced defects in the neurocranium, and the source for these cartilages are neural crest cells migrating anteriorly from the midbrain (Wada et al., 2005; Eberhart et al., 2006). Such cells have not been reported to undergo apoptosis in response to MO injection nor has a Class II-type midline defect been reported in association with MO artifacts (Robu et al., 2007; Gerety and Wilkinson, 2011). Second, during the course of our screen, mouse mutants for *Pkdcc* were reported and these animals were associated with cleft secondary palate, clearly providing further evidence for a function for these genes in craniofacial development (Imuta et al., 2009; Kinoshita et al., 2009). We also note that studies in mouse have indicated that the genetic or pharmacological lowering of p53 levels can ameliorate craniofacial phenotypes caused by mutations in *Tcof* or *Twsg* (Jones et al., 2008; Billington et al., 2011). These findings, together with our data, indicate that there are particular craniofacial phenotypes that require the presence of functional p53 protein. In support of this idea, the *Drosophila*

ortholog of *wu:fb16h09*, *nord*, has been shown to interact with p53 (Lunardi et al., 2010). In the future, based on our zebrafish findings, it would be of interest to determine if the clefting present in the *Pkdcc* knockout mouse model was similarly altered by a reduction of *p53*.

In summary, this MO-based screen has highlighted a set of conserved genes and gene families that influence the development and patterning of the zebrafish craniofacial skeleton. The function of these genes warrants further analysis that should extend beyond the zebrafish system, potentially including the reexamination of craniofacial development in existing mouse models.

Experimental Procedures

BLAST Analysis

To identify zebrafish orthologs, mouse candidate gene transcript and protein sequences were subjected to BLAST analysis (http://blast.ncbi.nlm.nih.gov/Blast.cgi) using the zebrafish RefSeq mRNA and protein databases. In some cases zebrafish genes were not readily identifiable. Here, we attempted to use a bootstrapping approach by identifying orthologs in other species using the *Takifugu rubripes*, *Xenopus laevis* and *X. tropicalis* databases followed by BLAST analysis of the zebrafish databases. This approach did not yield any additional hits than those already identified using a direct BLAST analysis of either the *Danio rerio* nucleotide or protein databases.

Zebrafish strains and Morpholino injections

Morpholinos were designed by Gene-Tools (Philomath, OR) based on the gene structure information we provided. Morpholinos (MOs) were resuspended in water prior to pressure injection into one-cell stage Zebrafish (*Danio rerio*) embryos. Initial injections were performed using a Morpholino dose range from 5-20ng with 2.5% tetramethylrhodamine dextran (#D1817, Invitrogen) as a tracer. Embryos were then raised at 28.5°C until 5 days post-fertilization (dpf) when they were fixed, photographed and processed for skeletal staining. The phenotypes of between 50-100 embryos were scored for each MO injected. The initial analysis of each Morpholino was performed in the wild-type TAB strain. Subsequent analysis of selected Morpholinos employed the *p53* mutant fish line, $tp53^{M214K}$, maintained on an AB background (Berghmans et al., 2005). Alternatively, experimental MOs were co-injected with a *p53*-specific MO (5′-GAC CTC CTC TCC ACT AAA CTA CGA T-3′) which was present at doses 2-fold higher than the MO targeted to the gene of interest (Robu et al., 2007).

RNA isolation, cDNA synthesis, RT-PCR and in situ hybridization

Whole embryo RNA pools were isolated from zebrafish at 24 and 48hpf using TRIzol extraction (Invitrogen, #15596-026; Carlsbad, CA) followed by a purification step using a Qiagen RNeasy RNA purification kit (#74104; Valencia, CA) both per manufacturer's protocols. cDNA pools were synthesized from whole embryo RNA using the Superscript III First-Strand Synthesis System (Invitrogen, #18080-051; Carlsbad, CA).

To detect changes in mRNA transcripts in morphant embryos, PCR was performed on cDNA pools using gene-specific primers that span the MO-targeted exon-intron boundaries. Primers were as follows: *smoc2* forward 5′-CCA GTG TGT TGG ACG CAT TAT CC-3′ and reverse 5′-GCG GGA ACA ATT ATA GCT CCC ACT TTA GCC-3′; *meis1* forward 5′-GAC TAA AGG AAG ACG AGG GAG TGT G-3′ and reverse 5′-CCT TC TCT GTC GTC TAT AAC CAAG TC-3′; *wu:fb16h09* forward 5′-GCA TCG TGC AGT TGT ACC CCG CCA GAA TGG GCC-3′ and reverse 5′-GCT CAG AGC TCT GTT GGT GGT GAG -3′; *macc1* forward 5′-GTT CGC TGA AAG ACT GAG TAG AGA AAC-3′ and either reverse R1 5′-GGA TTT GAC CTG CCC AGC TGA TTC C-3′ or reverse R2 5′-GAT GAG CTA CTA GCC CTT GAG CAT CCA TC-3′; pkdcc forward 5′- GGT CTG TCA AGA GGA CTC TGA CTG CCT GCT GCA G -3′ and reverse 5′- CAC ACA ACC CTG CTG TCT GTA CGA CGG CCA GCA TCG G -3′; *vgll4l* forward 5′- CCA GTC ATG GAC GAG CCT CTG G -3′ and reverse 5′- CGT CTA CAG ACA CGC TGA TGG AC -3′; β-actin forward 5′-CGA GCT GTC TTC CCA TCC A-3′, and reverse 5′-TCA CCA ACG TAG CTG TCT TTC TG-3′. PCR products were analyzed by agarose gel electrophoresis, then subcloned using the TOPO-blunt PCR cloning kit (Invitrogen #K2800-20) prior to sequencing using T7 and SP6 primers to identify specific transcript changes.

In situ hybridization (ISH) probe sequences were generated for wu:fb16h09, macc1, vlk, pkdcc, tshz2, pcdh19, and lix1l using PCR amplification from cDNA pools (see Supplementary Figure 3 for primer sequences). PCR products were subcloned using the TOPO-blunt PCR cloning kit (Invitrogen). Plasmids were linearized and antisense RNA probes synthesized with the appropriate RNA polymerase (see Supplementary Table 3) as previously described (Reid et al., 2010). A clone for *Adap1* was obtained from ZFIN (MGC: 92360) and the probe synthesized according to the associated documentation (Thisse 2004). In situ hybridization was performed on mouse and zebrafish embryos as described (Reid et al., 2010; Johnson et al., 2011).

Phenotypic Analysis

At 5dpf, zebrafish larvae were fixed in 4% paraformaldehyde in PBS for 2hrs and then transferred to a 50% ethanol solution and stored at 4°C. Fixed larvae were photographed prior to skeletal staining to determine gross facial phenotypes using a Leica M420 macroscope and SPOT RT3 camera. Alcian blue and alizarin red staining was performed as previously described (Walker and Kimmel, 2007). Cranial cartilages were photographed in whole mount as described above for the fixed larvae. Alternatively, the cartilages of the neurocranium (NC) and viscerocranium (VC) were separated using 0.005mm tip forceps and tungsten needles and flat mounted on glass slides in 20% glycerol, 0.25M potassium hydroxide. Flat mount prepared cartilages were photographed on a Nikon Eclipse E600 microscope and a SPOT RT Slider camera under 10X and 20X magnifications. Adobe Photoshop CS3 software was used to prepare images for publication.

Supplementary Material

Refer to Web version on PubMed Central for supplementary material.

Acknowledgments

The authors would like to thank members of the Artinger and Williams laboratories for help and advice, and David Stock and Tom Schilling for initial discussions concerning the screen.

This work is supported by NIH grant R21 DE018005 (T.W.) and P30 NIH NS048154 (K.A.)

References

Abouzeid H, Boisset G, Favez T, Youssef M, Marzouk I, Shakankiry N, Bayoumi N, Descombes P, Agosti C, Munier FL, Schorderet DF. Mutations in the SPARC-related modular calcium-binding protein 1 gene, SMOC1, cause waardenburg anophthalmia syndrome. Am J Hum Genet. 2011; 88:92–98. [PubMed: 21194680]

Amsterdam A, Burgess S, Golling G, Chen W, Sun Z, Townsend K, Farrington S, Haldi M, Hopkins N. A large-scale insertional mutagenesis screen in zebrafish. Genes Dev. 1999; 13:2713–2724. [PubMed: 10541557]

Berghmans S, Murphey RD, Wienholds E, Neuberg D, Kutok JL, Fletcher CD, Morris JP, Liu TX, Schulte-Merker S, Kanki JP, Plasterk R, Zon LI, Look AT. tp53 mutant zebrafish develop malignant peripheral nerve sheath tumors. Proc Natl Acad Sci U S A. 2005; 102:407–412. [PubMed: 15630097]

Billington CJ Jr. Ng B, Forsman C, Schmidt B, Bagchi A, Symer DE, Schotta G, Gopalakrishnan R, Sarver AL, Petryk A. The molecular and cellular basis of variable craniofacial phenotypes and their genetic rescue in Twisted gastrulation mutant mice. Dev Biol. 2011; 355:21–31. [PubMed: 21549111]

Biswas S, Emond MR, Jontes JD. Protocadherin-19 and N-cadherin interact to control cell movements during anterior neurulation. J Cell Biol. 2010; 191:1029–1041. [PubMed: 21115806]

Bloch-Zupan A, Jamet X, Etard C, Laugel V, Muller J, Geoffroy V, Strauss JP, Pelletier V, Marion V, Poch O, Strahle U, Stoetzel C, Dollfus H. Homozygosity mapping and candidate prioritization identify mutations, missed by whole-exome sequencing, in SMOC2, causing major dental developmental defects. Am J Hum Genet. 2011; 89:773–781. [PubMed: 22152679]

Brand M, Heisenberg CP, Warga RM, Pelegri F, Karlstrom RO, Beuchle D, Picker A, Jiang YJ, Furutani-Seiki M, van Eeden FJ, Granato M, Haffter P, Hammerschmidt M, Kane DA, Kelsh RN, Mullins MC, Odenthal J, Nusslein-Volhard C. Mutations affecting development of the midline and general body shape during zebrafish embryogenesis. Development. 1996; 123:129–142. [PubMed: 9007235]

Caubit X, Lye CM, Martin E, Core N, Long DA, Vola C, Jenkins D, Garratt AN, Skaer H, Woolf AS, Fasano L. Teashirt 3 is necessary for ureteral smooth muscle differentiation downstream of SHH and BMP4. Development. 2008; 135:3301–3310. [PubMed: 18776146]

Caubit X, Thoby-Brisson M, Voituron N, Filippi P, Bevengut M, Faralli H, Zanella S, Fortin G, Hilaire G, Fasano L. Teashirt 3 regulates development of neurons involved in both respiratory rhythm and airflow control. J Neurosci. 2010; 30:9465–9476. [PubMed: 20631175]

Chai Y, Maxson RE Jr. Recent advances in craniofacial morphogenesis. Dev Dyn. 2006; 235:2353–2375. [PubMed: 16680722]

Core N, Caubit X, Metchat A, Boned A, Djabali M, Fasano L. Tshz1 is required for axial skeleton, soft palate and middle ear development in mice. Dev Biol. 2007; 308:407–420. [PubMed: 17586487]

Crowley MA, Conlin LK, Zackai EH, Deardorff MA, Thiel BD, Spinner NB. Further evidence for the possible role of MEIS2 in the development of cleft palate and cardiac septum. Am J Med Genet A. 2010; 152A:1326–1327. [PubMed: 20425846]

Curtin E, Hickey G, Kamel G, Davidson AJ, Liao EC. Zebrafish wnt9a is expressed in pharyngeal ectoderm and is required for palate and lower jaw development. Mech Dev. 2011; 128:104–115. [PubMed: 21093584]

Dixon MJ, Marazita ML, Beaty TH, Murray JC. Cleft lip and palate: understanding genetic and environmental influences. Nat Rev Genet. 2011; 12:167–178. [PubMed: 21331089]

Eberhart JK, He X, Swartz ME, Yan YL, Song H, Boling TC, Kunerth AK, Walker MB, Kimmel CB, Postlethwait JH. MicroRNA Mirn140 modulates Pdgf signaling during palatogenesis. Nat Genet. 2008; 40:290–298. [PubMed: 18264099]

Eberhart JK, Swartz ME, Crump JG, Kimmel CB. Early Hedgehog signaling from neural to oral epithelium organizes anterior craniofacial development. Development. 2006; 133:1069–1077. [PubMed: 16481351]

Emond MR, Biswas S, Jontes JD. Protocadherin-19 is essential for early steps in brain morphogenesis. Dev Biol. 2009; 334:72–83. [PubMed: 19615992]

Feng W, Leach SM, Tipney H, Phang T, Geraci M, Spritz RA, Hunter LE, Williams T. Spatial and temporal analysis of gene expression during growth and fusion of the mouse facial prominences. PLoS One. 2009; 4:e8066. [PubMed: 20016822]

Ferretti E, Li B, Zewdu R, Wells V, Hebert JM, Karner C, Anderson MJ, Williams T, Dixon J, Dixon MJ, Depew MJ, Selleri L. A conserved Pbx-Wnt-p63-Irf6 regulatory module controls face morphogenesis by promoting epithelial apoptosis. Dev Cell. 2011; 21:627–641. [PubMed: 21982646]

Gerety SS, Wilkinson DG. Morpholino artifacts provide pitfalls and reveal a novel role for pro-apoptotic genes in hindbrain boundary development. Dev Biol. 2011; 350:279–289. [PubMed: 21145318]

Hammerschmidt M, Pelegri F, Mullins MC, Kane DA, Brand M, van Eeden FJ, Furutani-Seiki M, Granato M, Haffter P, Heisenberg CP, Jiang YJ, Kelsh RN, Odenthal J, Warga RM, Nusslein-Volhard C. Mutations affecting morphogenesis during gastrulation and tail formation in the zebrafish, Danio rerio. Development. 1996; 123:143–151. [PubMed: 9007236]

Horie K, Yusa K, Yae K, Odajima J, Fischer SE, Keng VW, Hayakawa T, Mizuno S, Kondoh G, Ijiri T, Matsuda Y, Plasterk RH, Takeda J. Characterization of Sleeping Beauty transposition and its application to genetic screening in mice. Mol Cell Biol. 2003; 23:9189–9207. [PubMed: 14645530]

Hu D, Marcucio RS. Unique organization of the frontonasal ectodermal zone in birds and mammals. Dev Biol. 2009; 325:200–210. [PubMed: 19013147]

Imuta Y, Nishioka N, Kiyonari H, Sasaki H. Short limbs, cleft palate, and delayed formation of flat proliferative chondrocytes in mice with targeted disruption of a putative protein kinase gene, Pkdcc (AW548124). Dev Dyn. 2009; 238:210–222. [PubMed: 19097194]

Johnson CW, Hernandez-Lagunas L, Feng W, Melvin VS, Williams T, Artinger KB. Vgll2a is required for neural crest cell survival during zebrafish craniofacial development. Dev Biol. 2011; 357:269–281. [PubMed: 21741961]

Jones NC, Lynn ML, Gaudenz K, Sakai D, Aoto K, Rey JP, Glynn EF, Ellington L, Du C, Dixon J, Dixon MJ, Trainor PA. Prevention of the neurocristopathy Treacher Collins syndrome through inhibition of p53 function. Nat Med. 2008; 14:125–133. [PubMed: 18246078]

Kimmel CB, Miller CT, Moens CB. Specification and morphogenesis of the zebrafish larval head skeleton. Dev Biol. 2001; 233:239–257. [PubMed: 11336493]

Kinoshita M, Era T, Jakt LM, Nishikawa S. The novel protein kinase Vlk is essential for stromal function of mesenchymal cells. Development. 2009; 136:2069–2079. [PubMed: 19465597]

Kuang XL, Zhao XM, Xu HF, Shi YY, Deng JB, Sun GT. Spatio-temporal expression of a novel neuron-derived neurotrophic factor (NDNF) in mouse brains during development. BMC Neurosci. 2010; 11:137. [PubMed: 20969804]

Lawson ND, Wolfe SA. Forward and reverse genetic approaches for the analysis of vertebrate development in the zebrafish. Dev Cell. 2011; 21:48–64. [PubMed: 21763608]

Liu P, Lu J, Cardoso WV, Vaziri C. The SPARC-related factor SMOC-2 promotes growth factor-induced cyclin D1 expression and DNA synthesis via integrin-linked kinase. Mol Biol Cell. 2008; 19:248–261. [PubMed: 17989364]

Liu P, Pazin DE, Merson RR, Albrecht KH, Vaziri C. The developmentally-regulated Smoc2 gene is repressed by Aryl-hydrocarbon receptor (Ahr) signaling. Gene. 2009; 433:72–80. [PubMed: 19146932]

Lunardi A, Di Minin G, Provero P, Dal Ferro M, Carotti M, Del Sal G, Collavin L. A genome-scale protein interaction profile of Drosophila p53 uncovers additional nodes of the human p53 network. Proc Natl Acad Sci U S A. 2010; 107:6322–6327. [PubMed: 20308539]

Maier S, Paulsson M, Hartmann U. The widely expressed extracellular matrix protein SMOC-2 promotes keratinocyte attachment and migration. Exp Cell Res. 2008; 314:2477–2487. [PubMed: 18582461]

Moens CB, Selleri L. Hox cofactors in vertebrate development. Dev Biol. 2006; 291:193–206. [PubMed: 16515781]

Moore FE, Reyon D, Sander JD, Martinez SA, Blackburn JS, Khayter C, Ramirez CL, Joung JK, Langenau DM. Improved somatic mutagenesis in zebrafish using transcription activator-like effector nucleases (TALENs). PLoS One. 2012; 7:e37877. [PubMed: 22655075]

Neuhauss SC, Solnica-Krezel L, Schier AF, Zwartkruis F, Stemple DL, Malicki J, Abdelilah S, Stainier DY, Driever W. Mutations affecting craniofacial development in zebrafish. Development. 1996; 123:357–367. [PubMed: 9007255]

Okada I, Hamanoue H, Terada K, Tohma T, Megarbane A, Chouery E, Abou-Ghoch J, Jalkh N, Cogulu O, Ozkinay F, Horie K, Takeda J, Furuichi T, Ikegawa S, Nishiyama K, Miyatake S, Nishimura A, Mizuguchi T, Niikawa N, Hirahara F, Kaname T, Yoshiura K, Tsurusaki Y, Doi H, Miyake N, Furukawa T, Matsumoto N, Saitsu H. SMOC1 is essential for ocular and limb development in humans and mice. Am J Hum Genet. 2011; 88:30–41. [PubMed: 21194678]

Piotrowski T, Schilling TF, Brand M, Jiang YJ, Heisenberg CP, Beuchle D, Grandel H, van Eeden FJ, Furutani-Seiki M, Granato M, Haffter P, Hammerschmidt M, Kane DA, Kelsh RN, Mullins MC, Odenthal J, Warga RM, Nusslein-Volhard C. Jaw and branchial arch mutants in zebrafish II: anterior arches and cartilage differentiation. Development. 1996; 123:345–356. [PubMed: 9007254]

Popperl H, Rikhof H, Chang H, Haffter P, Kimmel CB, Moens CB. lazarus is a novel pbx gene that globally mediates hox gene function in zebrafish. Mol Cell. 2000; 6:255–267. [PubMed: 10983974]

Rainger J, van Beusekom E, Ramsay JK, McKie L, Al-Gazali L, Pallotta R, Saponari A, Branney P, Fisher M, Morrison H, Bicknell L, Gautier P, Perry P, Sokhi K, Sexton D, Bardakjian TM, Schneider AS, Elcioglu N, Ozkinay F, Koenig R, Megarbane A, Semerci CN, Khan A, Zafar S, Hennekam R, Sousa SB, Ramos L, Garavelli L, Furga AS, Wischmeijer A, Jackson IJ, Gillessen-Kaesbach G, Brunner HG, Wieczorek D, van Bokhoven H, Fitzpatrick DR. Loss of the BMP antagonist, SMOC-1, causes Ophthalmo-acromelic (Waardenburg Anophthalmia) syndrome in humans and mice. PLoS Genet. 2011; 7:e1002114. [PubMed: 21750680]

Reid BS, Sargent TD, Williams T. Generation and characterization of a novel neural crest marker allele, Inka1-LacZ, reveals a role for Inka1 in mouse neural tube closure. Dev Dyn. 2010; 239:1188–1196. [PubMed: 20175189]

Robu ME, Larson JD, Nasevicius A, Beiraghi S, Brenner C, Farber SA, Ekker SC. p53 activation by knockdown technologies. PLoS Genet. 2007; 3:e78. [PubMed: 17530925]

Rocnik EF, Liu P, Sato K, Walsh K, Vaziri C. The novel SPARC family member SMOC-2 potentiates angiogenic growth factor activity. J Biol Chem. 2006; 281:22855–22864. [PubMed: 16774925]

Santos JS, Fonseca NA, Vieira CP, Vieira J, Casares F. Phylogeny of the teashirt-related zinc finger (tshz) gene family and analysis of the developmental expression of tshz2 and tshz3b in the zebrafish. Dev Dyn. 2010; 239:1010–1018. [PubMed: 20108322]

Schilling TF, Kimmel CB. Segment and cell type lineage restrictions during pharyngeal arch development in the zebrafish embryo. Development. 1994; 120:483–494. [PubMed: 8162849]

Schilling TF, Le Pabic P. Fishing for the signals that pattern the face. J Biol. 2009; 8:101. [PubMed: 20067597]

Schilling TF, Piotrowski T, Grandel H, Brand M, Heisenberg CP, Jiang YJ, Beuchle D, Hammerschmidt M, Kane DA, Mullins MC, van Eeden FJ, Kelsh RN, Furutani-Seiki M, Granato M, Haffter P, Odenthal J, Warga RM, Trowe T, Nusslein-Volhard C. Jaw and branchial arch mutants in zebrafish I: branchial arches. Development. 1996; 123:329–344. [PubMed: 9007253]

Selleri L, Depew MJ, Jacobs Y, Chanda SK, Tsang KY, Cheah KS, Rubenstein JL, O'Gorman S, Cleary ML. Requirement for Pbx1 in skeletal patterning and programming chondrocyte proliferation and differentiation. Development. 2001; 128:3543–3557. [PubMed: 11566859]

Stein U, Walther W, Arlt F, Schwabe H, Smith J, Fichtner I, Birchmeier W, Schlag PM. MACC1, a newly identified key regulator of HGF-MET signaling, predicts colon cancer metastasis. Nat Med. 2009; 15:59–67. [PubMed: 19098908]

Swartz ME, Sheehan-Rooney K, Dixon MJ, Eberhart JK. Examination of a palatogenic gene program in zebrafish. Dev Dyn. 2011; 240:2204–2220. [PubMed: 22016187]

Szabo-Rogers HL, Smithers LE, Yakob W, Liu KJ. New directions in craniofacial morphogenesis. Dev Biol. 2010; 341:84–94. [PubMed: 19941846]

Thisse, B.; Pflumio, S.; Fürthauer, M.; Loppin, B.; Heyer, V.; Degrave, A.; Woehl, R.; Lux, A.; T., S.; Charbonnier, XQ.; Thisse, C. Expression of the zebrafish genome during embryogenesis (NIH R01 RR15402). ZFIN Direct Data Submission. 2001.

Thisse, C.; Thisse, B. High Throughput Expression Analysis of ZF-Models Consortium Clones ZFIN Direct Data Submission. 2005.

Vannahme C, Gosling S, Paulsson M, Maurer P, Hartmann U. Characterization of SMOC-2, a modular extracellular calcium-binding protein. Biochem J. 2003; 373:805–814. [PubMed: 12741954]

Volff JN. Genome evolution and biodiversity in teleost fish. Heredity (Edinb). 2005; 94:280–294. [PubMed: 15674378]

Wada N, Javidan Y, Nelson S, Carney TJ, Kelsh RN, Schilling TF. Hedgehog signaling is required for cranial neural crest morphogenesis and chondrogenesis at the midline in the zebrafish skull. Development. 2005; 132:3977–3988. [PubMed: 16049113]

Walker MB, Kimmel CB. A two-color acid-free cartilage and bone stain for zebrafish larvae. Biotech Histochem. 2007; 82:23–28. [PubMed: 17510811]

Wang D, Jao LE, Zheng N, Dolan K, Ivey J, Zonies S, Wu X, Wu K, Yang H, Meng Q, Zhu Z, Zhang B, Lin S, Burgess SM. Efficient genome-wide mutagenesis of zebrafish genes by retroviral insertions. Proc Natl Acad Sci U S A. 2007; 104:12428–12433. [PubMed: 17640903]

Weiner AM, Scampoli NL, Calcaterra NB. Fishing the molecular bases of Treacher Collins syndrome. PLoS One. 2012; 7:e29574. [PubMed: 22295061]

Yan YL, Willoughby J, Liu D, Crump JG, Wilson C, Miller CT, Singer A, Kimmel C, Westerfield M, Postlethwait JH. A pair of Sox: distinct and overlapping functions of zebrafish sox9 co-orthologs in craniofacial and pectoral fin development. Development. 2005; 132:1069–1083. [PubMed: 15689370]

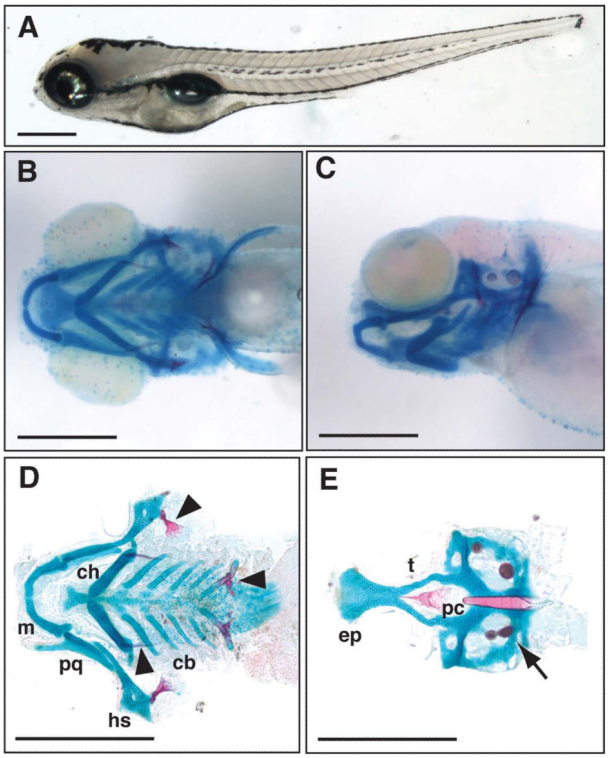

Figure 1.

External morphology and craniofacial cartilage organization in wild-type 5 day post-fertilization (dpf) *Danio rerio* larvae. A, lateral view of a fixed zebrafish larva. B, ventral view of larval head skeleton. C, lateral view of same fish imaged in B. D, flat-mount of viscerocranial skeleton after removal of the neurocranium (10X magnification). E, flat-mount of neurocranium (10X magnification). cb, ceratobranchials; ch, ceratohyal; ep, ethmoid plate; hs, hyosymplectic; m, Meckel's; pc, parachordals; pq, palatoquadrate; and t, trabecula. Bone and pharyngeal teeth (arrowheads) and otic vesicles (arrow) are also shown. Scale bars are 500μm.

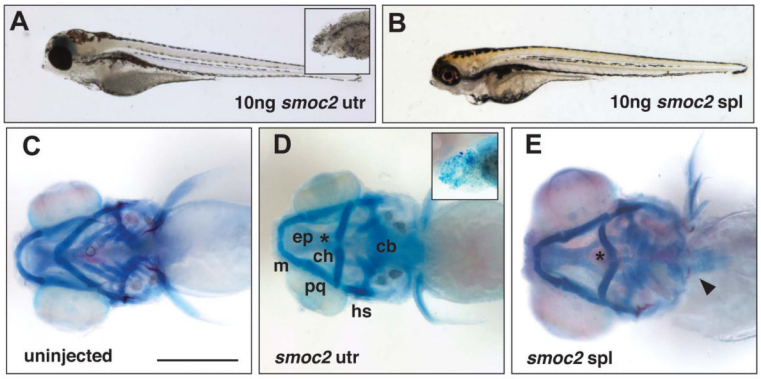

Figure 2.

Defects in the viscerocranium of Class I *smoc2* morphants. A, lateral view of 5dpf zebrafish larva injected with 10ng *smoc2* UTR Morpholino; inset more severe *smoc2* morphant with severely reduced head. B, lateral view of 5dpf zebrafish larva injected with 10ng *smoc2* SPL Morpholino. C, ventral view of the craniofacial skeleton of an uninjected larva at 5dpf. D, ventral view of the cranial skeleton of a *smoc2* UTR morphant at 5dpf; inset shows lack of discrete craniofacial cartilages in severe *smoc2* UTR morphant. E, ventral view of the cranial skeleton of a *smoc2* SPL morphant. Asterisk denotes flattened or inverted ceratohyal and arrowhead indicates the presence of pharyngeal teeth in some *smoc2* morphants. Abbreviations as in Figure 1.

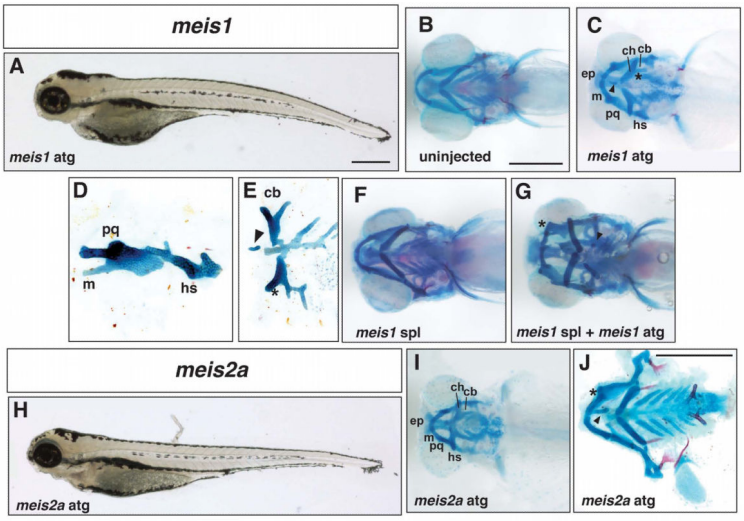

Figure 3.

Defects in cranial development in Class I *meis* morphants. A, lateral view of a 5dpf larva injected with 5ng *meis1* ATG Morpholino. B, ventral view of the craniofacial skeleton of an uninjected larva at 5dpf. C, ventral view of a *meis1* ATG morphant showing a fusion between the Meckel's and palatoquadrate cartilages and the ceratohyal and first ceratobranchial (asterisk). Ectopic cartilage is indicated by an arrowhead. D, lateral view of a flat mount showing a fused Meckel's and palatoquadrate cartilage and the hyosymplectic. E, ventral view of flat mount showing ectopic cartilage (arrowhead) and fused ceratobranchials (asterisk). F, ventral view of a larval skeleton 5 days after injection with 20ng *meis1* SPL Morpholino. G, ventral view of a larval skeleton after co-injection with 20ng *meis1* SPL Morpholino and 2ng *meis1* ATG Morpholino. Ectopic cartilage is indicated by an arrowhead and the fusion between Meckel's and the palatoquadrate is indicated by the asterisk. H, lateral view of a 5dpf larva injected with 10ng *meis2a* Morpholino. I, ventral view of the skeleton of a *meis2a* ATG morphant. J, flat mount of a *meis2a* morphant (5ng ATG MO) indicating a fusion between Meckel's and palatoquadrate (asterisk) and ectopic cartilage (arrowhead). Abbreviations as in Figure 1.

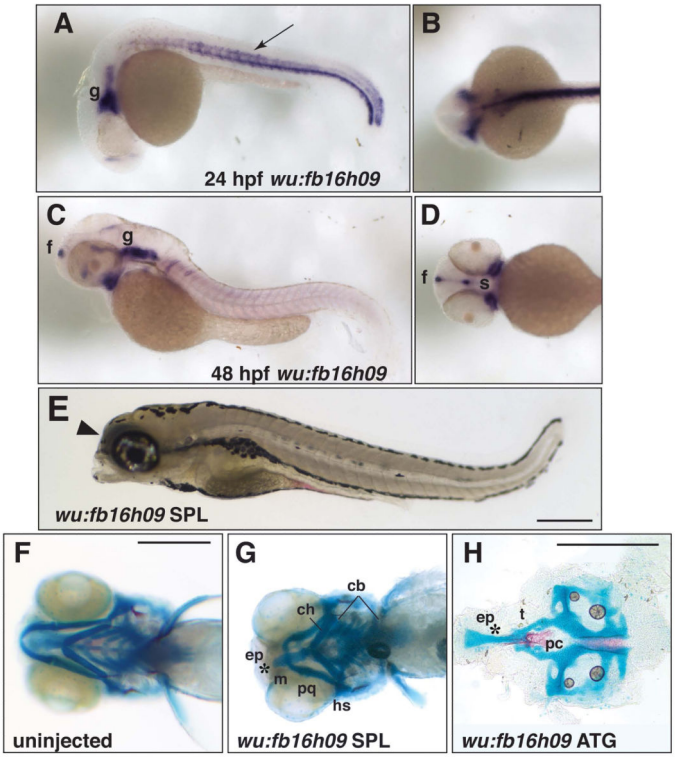

Figure 4.

Neurocranium defects elicited by knock-down of *wu:fb16h09*. A-D, in situ hybridization for expression of *wu:fb16h09.* A, lateral view and B, dorsal view of a 24hpf embryo showing expression of *wu:fb16h09* in neural tissues of the head (g; ganglia) and trunk hypochord, middle of the somite and ventral spinal cord (arrow). C, lateral view and D, ventral view of a 48hpf zebrafish showing expression of *wu:fb16h09* in the forebrain (f), trigeminal and other cranial ganglion (g) and regions flanking the presumptive mouth (s, stomodeum). E, lateral view of a 5dpf larva after injection with 10ng *wu:fb16h09* Morpholino. Arrowhead indicates collapse of the head rostral to the eye. F, ventral view of the craniofacial skeleton of an uninjected larva at 5dpf. G, ventral view of 5dpf skeleton of a *wu:fb16h09* SPL morphant showing loss of the ethmoid plate and fusion of the trabeculae. (Note that we do not observe cartilage fusions in the viscerocranium with this Morpholino). H, flat mount of the neurocranium of *wu:fb16h09* ATG morphant after injection with 10ng ATG Morpholino. Asterisk indicates reduced/absent ethmoid plate and fused trabeculae. Other abbreviations as in Figure 1.

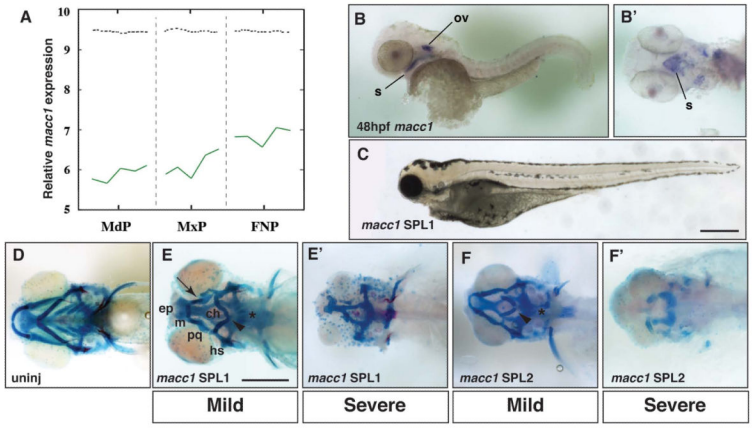

Figure 5.

Analysis of *macc1* expression and function in the larval zebrafish head. A, Microarray analysis of *Macc1* expression in the embryonic mouse face. Expression increases in the mandibular (MdP), maxillary (MxP) and frontonasal (FNP) prominences between E10.5 to E12.5. The x-axis represents the five time points for each prominence. The y-axis shows the relative expression level on a $\log_2$ scale – i.e. every integer represents a doubling in the level of expression from the preceding number. The dashed black line indicates the average expression level for all probes. B, *In situ* hybridization for *macc1* at 48hpf. Lateral view shows *macc1* expression in the otic vesicle (ov) and developing mouth (s). B', ventral view after removal of the yolk to more clearly show *macc1* expression in the roof of the stomodeum (s). C, lateral view of 5dpf zebrafish after injection of 7.5ng *macc1* SPL1. The head and eyes of *macc1* morphants are hypoplastic. D, ventral view of the craniofacial skeleton of an uninjected larva at 5dpf. E, ventral view of mild phenotypes associated with injection of 5ng *macc1* SPL1 Morpholino. E', ventral view of severe phenotypes associated with injection of 10ng SPL1 *macc1* Morpholino. F, ventral view of mild phenotypes associated with injection of 10ng *macc1* SPL2 Morpholino. F', ventral view of severe phenotypes associated with injection of 20ng SPL2 *macc1* Morpholino. Defects in the ceratobranchials (asterisk), the ceratohyals (arrowhead), and Meckel's and palatoquadrate cartilages resulting in a recessed lower jaw (arrow) are indicated. Other abbreviations as in Figure 1.

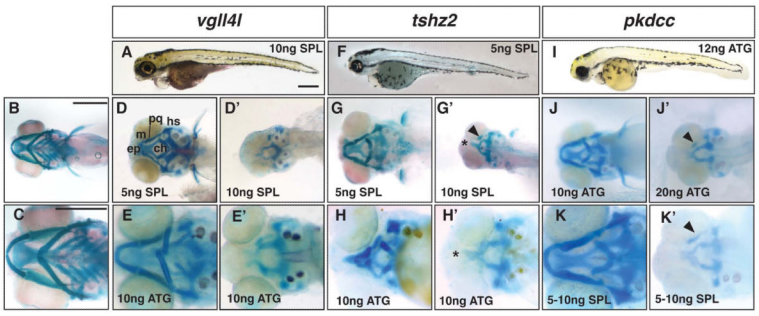

Figure 6.

Progressive and dose-dependent loss of the neural crest-derived cranial skeleton in Class III morphants. A, D-E', *vgll4l* morphants. F-H', *tshz2* morphants, I-K', *pkdcc* morphants. A, F, I, lateral view of 5dpf zebrafish after injection with gene-specific Morpholino. B and C, ventral view of uninjected larva at 5dpf. D, E, G, H, J, and K, ventral view of mild morphant phenotypes at 5dpf. D', E', G', H', J', and K', ventral view of severe morphant phenotypes. Lower panels are magnified images of craniofacial skeletons. Dose and Morpholino are indicated in the figure. The arrowheads in G', J' and K' indicate the remnants of the viscerocranial cartilages. Asterisk indicates fused trabecula and reduction of the ethmoid plate. Scale bars are 500μm in A, B, and C. Abbreviations as in Figure 1.

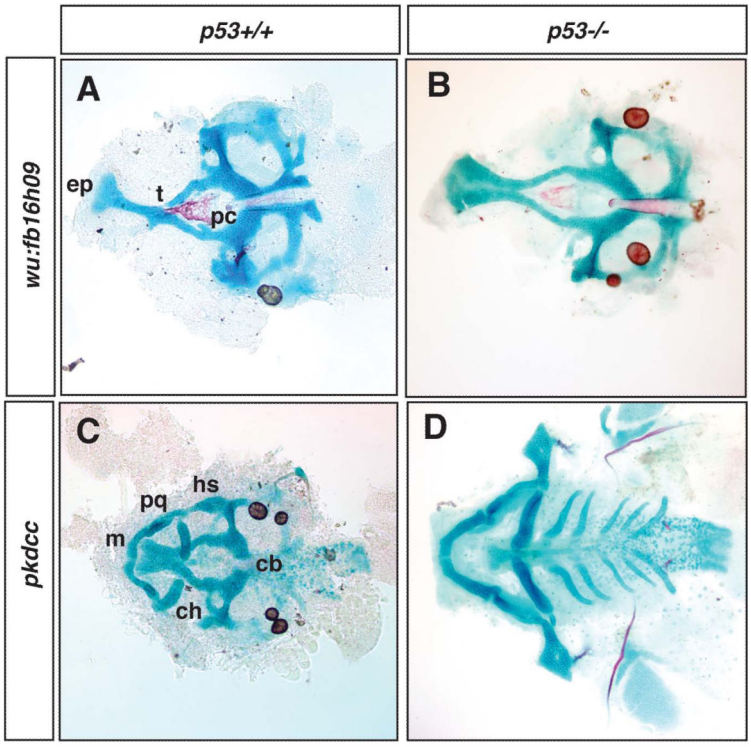

Figure 7.

Absence of *p53* alleviates the cartilage phenotypes present in *wu:fb16h09* and *pkdcc* morphants. A, flat-mounted neurocranium of *wu:fb16h09* morphant in wildtype zebrafish after injection of 10ng ATG Morpholino. B, flat-mounted neurocranium of *wu:fb16h09* morphant in *p53* null zebrafish after injection of 10ng ATG Morpholino. (Note that the *wu:fb16h09* ATG Morpholino only generates neurocranial defects and so we were not able to assess the influence of p53 on viscerocranial defects in this experiment). C, flat-mounted cranial cartilages of *pkdcc* morphant in wildtype zebrafish after injection of 20ng ATG Morpholino. D, flat-mounted cranial cartilages of *pkdcc* morphant in *p53* null zebrafish after injection of 20ng ATG Morpholino. Abbreviations as in Figure 1.

Table 1

Mouse genes and the Zebrafish orthologs (zebrafish nomenclature in brackets if different from mouse) that produced consistent craniofacial phenotypes when targeted with the indicated Morpholino sequences.

Gene Name	Mouse Accession ID	Zebrafish Accession ID	MO sequence	p53 Dependent MO Phenotype
Class I				
Smoc2	NM_022315	JQ085591	SPL AGGAAACAGTGAGACTCACCCTCTT UTR GCAGCTCCCCAGAAGCAGAAAATCC	No
Meis1	NM_010789 NM_001193271	NM_131893	ATG TATATCTTCGTACCTCTGCGCCATC SPL2 AAACTTTTCGGGATACGTACCCTCT	No
Meis2 (Meis2a)	NM_001159568	NM_131896	ATG CAGCTCATCGTACCTTTGCGCATC	No
Class II				
Ndnf (wu:fb16h09)	NM_172399	XM_684842	ATG ATAACATCCACACCTCCACGTCATC SPL CTGGCTCACCTAAGACACAGGAAAC	Yes
Class III				
Macc1	NM_001163136	NM_001199766	SPL1 CACAGCCCCCTAAGACAGACAAAAA SPL2 GAGAGCATAATTACCATGTAGGTTG	No
Vgll4 (Vgll4l)	NM_177683	NM_001079998	ATG TAGTGGAAATTAGTGACCGCCATTC SPL3 AGCTGTGGAGATACAATCAGATAGA	No
Tshz2	NM_080455	XM_002666523	ATG CCGCCTGTGCCACTTTCAGCAGCAT SPL GTATGCTGGAAACAGAACAGACAGA	No
Pkdcc (LOC565254)	NM_134117	XM_688532	ATG AACGGACTTCTTTGGAAAGTCATGG SPL2 ATGGAGATGAAAACTCACCCGTGGC	Yes